Neuroradiology (2007) 49:849–863
DOI 10.1007/s00234-007-0267-4

FUNCTIONAL NEURORADIOLOGY

Anatomical parcellation of the brainstem and cerebellar white matter: a preliminary probabilistic tractography study at 3 T

Christophe Habas · Emmanuel Alain Cabanis

Received: 30 January 2007 / Accepted: 4 June 2007 / Published online: 15 August 2007

Abstract
Introduction The aims of this study were: (1) to test whether higher spatial resolution diffusion tensor images and a higher field strength (3 T) enable a more accurate delineation of the anatomical tract within the brainstem, and, in particular, (2) to try to distinguish the different components of the corticopontocerebellar paths in terms of their cortical origins.
Methods The main tracts of the brainstem of four volunteers were studied at 3 T using a probabilistic diffusion tensor imaging (DTI) axonal tracking. The resulting tractograms enabled anatomical well-delineated structures to be identified on the diffusion tensor coloured images.
Results We tracked corticopontine, corticospinal, central tegmental, inferior and superior cerebellopeduncular, transverse, medial lemniscal and, possibly, longitudinal medial fibres. Moreover, DTI tracking allowed a broad delineation of the corticopontocerebellar paths.
Conclusion Diffusion tensor coloured images allow a rapid and reliable access to the white matter broad parcellation of the brainstem and of the cerebellum, which can be completed by fibre tracking. However, a more accurate and exhaustive depiction of the anatomical connectivity within the brainstem requires the application of more sophisticated techniques and tractography algorithms, such as diffusion spectrum imaging.

Keywords Diffusion tensor imaging · Probabilistic tractography · Brainstem · Cerebellum

C. Habas (✉) · E. A. Cabanis
Service de NeuroImagerie, Hôpital des Quinze-Vingts,
UPMC Paris 6,
28, rue de Charenton,
75012 Paris, France
e-mail: chabas@quinze-vingts.fr

Introduction

Diffusion tensor resonance magnetic imaging (DTI) and tractography allow the main constitutive anatomical tracts of the white matter in humans to be delineated in vivo. These methods have been successfully applied to the brainstem at 1.5 T [1–4] and at 3 T [5, 6]. Most of these studies identified the anatomical tracts by comparing the colour-coded maps generated from their data with a brain atlas. However, the discrimination of these techniques mainly depends upon the spatial resolution of the data, and upon the characteristics of the tractography algorithm used to compute the white matter pathways. Moreover, no attempt to depict the different components of the corticopontocerebellothalamic system as a function of their cortical origins has been made.

Therefore, we chose to reassess the white matter architecture of the brainstem at 3 T using high-resolution diffusion-weighted images ($1.05 \times 1.05 \times 1.00$ mm for the brainstem alone and $1.05 \times 1.05 \times 1.7$ mm for the whole brain), and a probabilistic tractography algorithm. Millimetric slices and probabilistic tractography allow thinner tracts within the brainstem to be identified and erratic computed trajectories determined, especially within low anisotropic areas, as in tegmental regions, respectively. In order to identify the cortical origins of cerebropontine projections, we completed and matched tractograms processed within the brainstem on millimetric slices with tractograms reconstructed over the whole brain.

Material and methods

Four young healthy subjects (two men and two women) were studied using a whole-body 3 T clinical imager (Signa

Horizon; General Electric Healthcare, Milwaukee, Wis.) with an eight-channel head coil. The DTI sequence was a diffusion-weighted single-shot spin-echo, echo-planar sequence (TE/TR 76.1/9,000 ms, FOV 26×26, matrix 128×128 zero-filled to 256×256, thickness 1 or 1.7 mm, interslice gap 0 mm, bandwidth 71.94 Hz, b 0 and 1,000 s/mm^2, NEX 2). The ASSET option was used in order to decrease acquisition time and image distortions of the posterior fossa. For the high value of b, two groups must be distinguished: (1) in two subjects, diffusion gradients were applied in 25 different directions, and in each single scan 72 contiguous axial slices (thickness 1 mm) were obtained to include the whole brainstem and the cerebellum, and (2) in two subjects, diffusion gradients were applied in 30 different directions, and, in each single scan 69 contiguous axial slices (thickness 1.7 mm) were obtained to include the whole brain, brainstem and the cerebellum.

DTI postprocessing was performed with the tools of the FMRIB software library (FSL, version 3.3; Oxford Centre for Functional MRI of the Brain, UK; http://www.fmrib.ox;ac;uk/fsl), and included: data transfer, format conversion, eddy current and motion artefact correction, local modelling of diffusion parameters and probabilistic fibre tracking. Probabilistic tractography estimates the most probable location of a pathway from a seed mask using the anisotropic volume fraction and applying Bayesian techniques [7]. The fibre-tracking algorithm was initiated from a seed mask positioned over the region of interest determined from the structural anisotropic image. From all voxels within a seed mask, the tractography algorithm generated 10,000 streamline samples, with a step length of 0.5 mm and a curvature threshold of 0.2. These samples were computed through the probability estimate on fibre direction at each voxel. Finally, the probability of a course within a given pixel was represented by the sum of these samples passing through it, and was colour-coded (yellow – low probability, red – high probability). We used a threshold of >30 samples to reject voxels with a low connectivity probability. Voxel values were laid over the corresponding fractional anisotropic images (structural images).

Seed points were located according to known anatomy as described in a brain atlas [8, 9], a cerebellum atlas [10], and a previous fibre tract-based atlas of the white matter [1–6]. Monovoxel seed points were preferred in order to optimize specificity of the fibre tracking. In a second procedure, a larger seed mask were used. Several easily delineated regions of interest were chosen to launch the tracking: (1) medullary olivary and red nuclei (for the central tegmental tract), (2) medullary pyramids (for the pyramidal tract), (3) restiform area within the dorsal medulla oblongata (for the inferior cerebellar peduncle), (4) medullary interolivary area (for the lemniscus medialis), (5) dentate nucleus (for the superior cerebellar peduncle), (7) deep white matter of the neocerebellar folia (for cerebellar afferents), (8) basis pontis (for transverse fibres), (9) crus cerebri (for corticopontine and corticospinal projections), and (10) trigeminal nerve. The exact course and target of the computed tract were compared with known anatomy to ensure their identity. For example, cortical afferents were recognized by their cortical origin, their position within the internal capsule and their target.

Results

Computed tractograms were identical in all the subjects studied.

The central tegmental tract

Rubroolivary fibres The computed course emanated from the principal nucleus of the inferior olivary nucleus (Fig. 1a,g). It ran caudodorsally and paramedially within the floor of the fourth ventricle, i.e. within the dorsal pontine tegmentum dorsal to the medial lemniscus, medial to the middle cerebellar peduncle and ventral to the inferior cerebellar peduncle (Fig. 1b,c). At the mesencephalodiencephalic level, its course remained ventral to the superior cerebellar peduncle and ran parallel to it within the mesencephalic tegmentum (Fig. 1d). Then, the course passed in a more ventral and medial position within the ventral tegmental decussation area (Fig. 1e) before reaching the ipsilateral red nucleus (Fig. 1f).

Corticoolivary fibres A second course is traced from the inferior olivary nucleus (Fig. 2a) and from its hilus (Fig. 2b), and runs in a strictly medially within the floor of the fourth ventricle (Fig. 2c,d). It goes through the mesencephalic tegmentum, lateral to the ventral decussation area, and reaches the most paramedial part of the ipsilateral crus cerebri (Fig. 2e). This bundle travels from the rostral part of the posterior limb (Fig. 2f) to the anterior limb of the internal capsule (Fig. 2g). It terminates within the dorsolateral part of the prefrontal cortex (Fig. 2h).

The inferior cerebellar peduncle

The course is traced within the dorsolateral part of the medulla oblongata (Fig. 3a). It ascends in the vicinity of but dorsal to the inferior olivary nucleus (Fig. 3b) before reaching more laterally the ipsilateral restiform body (Fig. 3c). The tract enters the cerebellar white matter dorsally to the central tegmental tract, ventrally to the superior cerebellar tract, and between the lateral wall of the

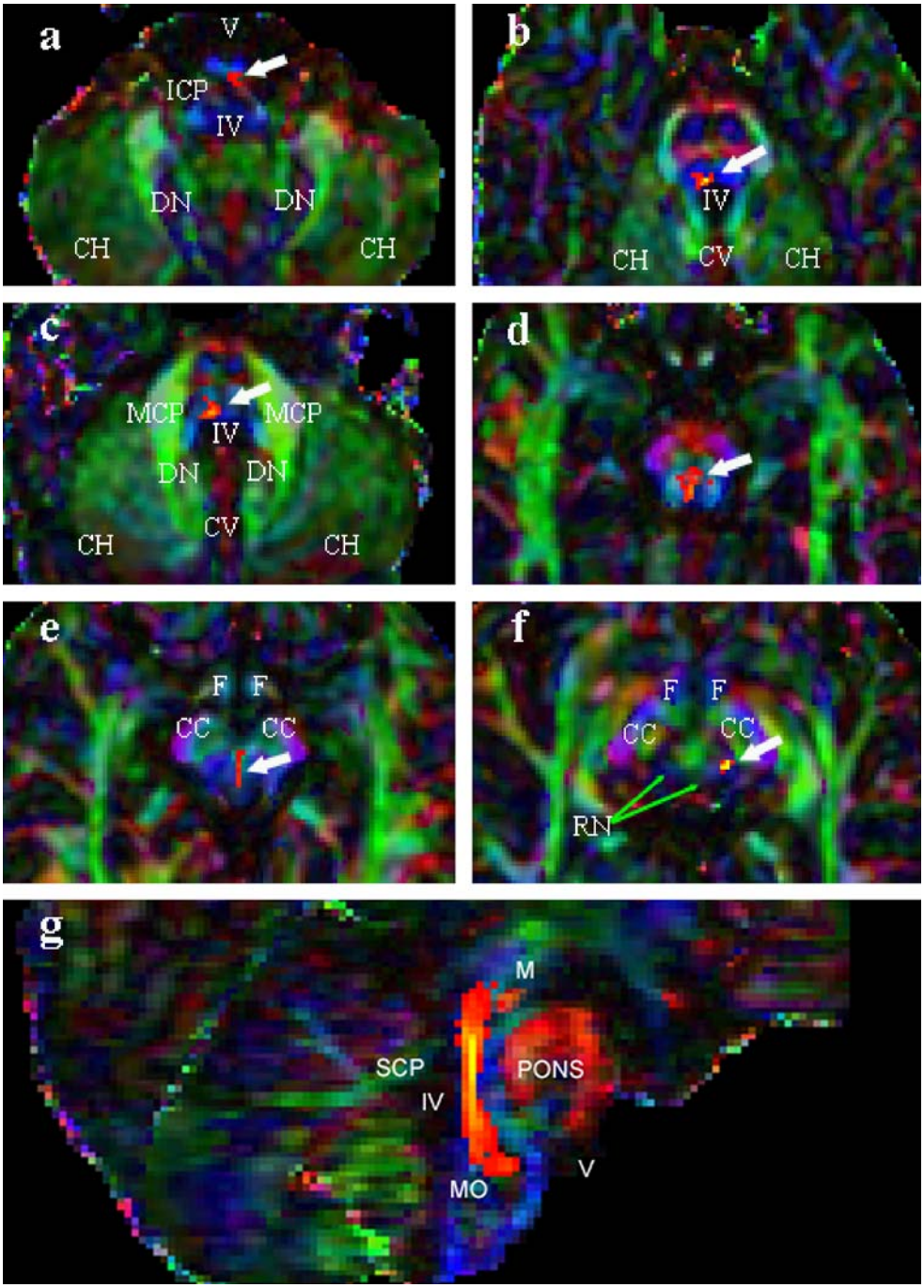

Fig. 1 Probabilistic mapping of the central tegmental tract: rubro-olivary part. In all images, only a suprathreshold probability of connections (>30 samples) are represented, and are overlaid on the anisotropic fraction images of one volunteer in an axial plane. On the coloured maps, *red*, *green* and *blue* represent fibres running along the laterolateral, ventrodorsal and rostrocaudal axes, respectively. In all images, reconstructed tracts are coloured according to their probability(*red* low, *yellow* high) and are indicated by a *thick white arrow*. **a** View at the medullary level. **b**–**d** View at the pontine level. **e** View at the mesencephalic level. **f** View at the mesencephalodiencephalic junction. **g** Paramedial view showing the tract going through the whole brainstem. **d** View showing prefrontorubral connections through the anterior limb of the internal capsule. **e**, **f** Views showing frontorubral and pericentrorubral connections. Well-delineated anatomic landmarks are labelled as follows: *CC* crus cerebri, *CH* cerebellar hemisphere, *CV* cerebellar vermis, *DN* dentate nucleus, *F* fornix, *ICP* inferior cerebellar peduncle, *IV* fourth ventricle, *M* mesencephalon, *MCP* middle cerebellar peduncle, *MO* medulla oblongata, *PONS* pons, *RN* red nucleus, *SCP* superior cerebellar peduncle, *TEC* tectum, *V* ventral

fourth ventricle and the middle cerebellar peduncle (Fig. 3d). Then the course runs within the cerebellar white matter above the dentate nucleus (Fig. 3e,f) and reaches the vermis and paravermis of the cerebellar anterior lobe (Fig. 3g,h), especially in lobules IV–VI and IX.

Transverse fibres and the middle cerebellar peduncle

Transverse fibres appear on structural anisotropic axial images as a large H-shaped red areas of the pons, circumscribing the two corticospinal tracts (blue; Fig. 4a). Morphologically, we can distinguish: ventral transverse fibres, medial fibres between the two corticospinal tracts, and dorsal fibres. These fibres can more precisely be subdivided in a laminar way according to their main respective cerebellar targets (Fig. 4a,b). Ventroventral fibres (Fig. 4a,b; arrow 1), medioventral fibres (arrow 2) and dorsoventral fibres (arrow 3) are connected to the lateral hemispheric part of lobules VIIIB, VIIIA, VII and VI, respectively (Fig. 4b–e). All these fibres converge caudally and constitute part of the middle cerebellar peduncle. Their course remains lateral and ventrolateral to the ipsilateral dentate nucleus. The dorsal fibres (Fig. 4a; arrow 4) gather

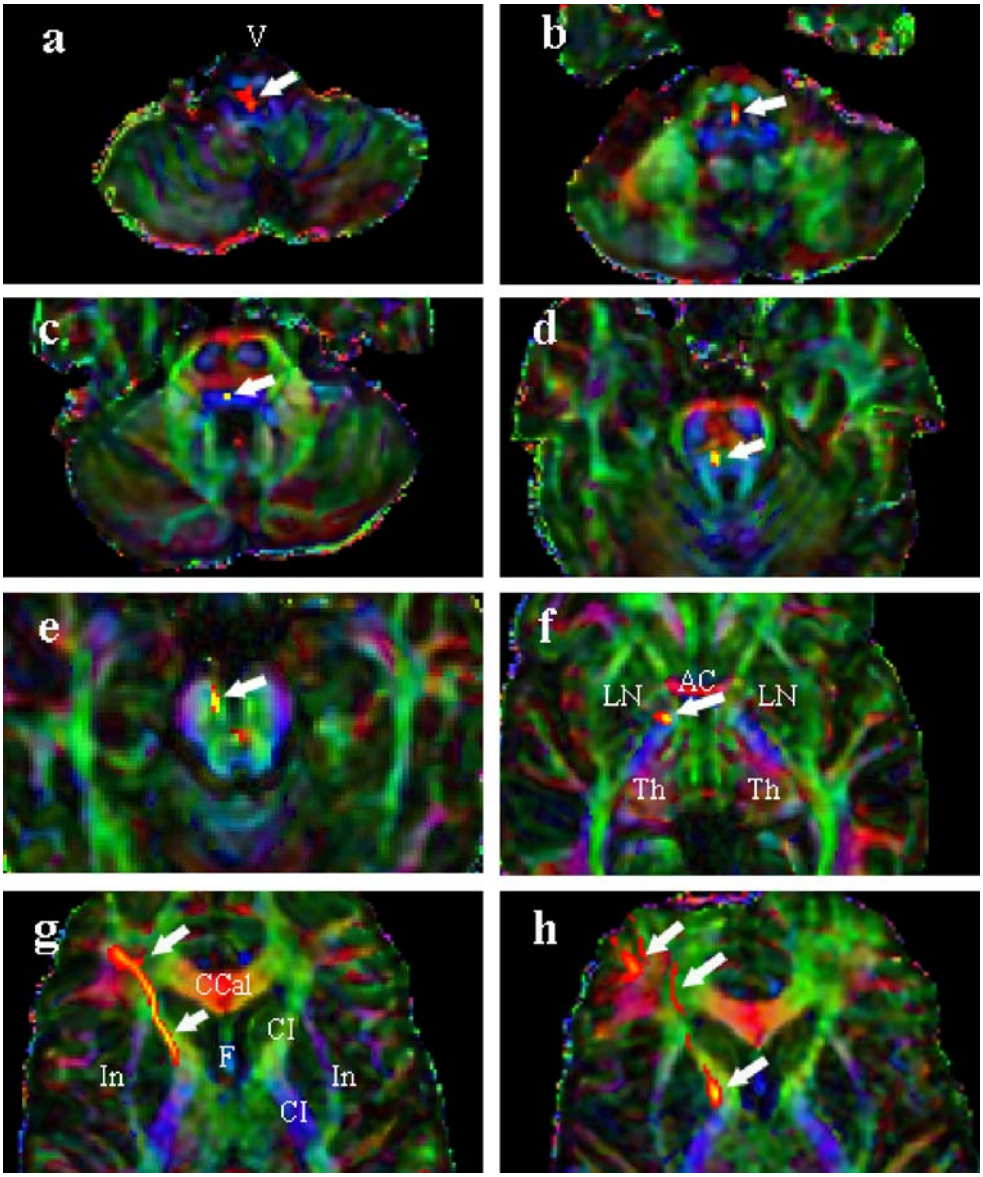

Fig. 2 Probabilistic mapping of the central tegmental tract: prefrontoolivary part. **a** View at the medullary level. **b**–**d** View at the pontine level. **e** View at the mesencephalic level. **f** View at the diencephalic level within the posterior part of the internal capsule. **g** View at the diencephalotelencephalic level within the anterior part of the internal capsule. **h** View at the telencephalic level. Well-delineated anatomic landmarks are labelled as follows: *AC* anterior commissure, *CCal* corpus callosum, *CH* cerebellar hemisphere, *F* fornix, *In* insula, *LN* lentiform nucleus, *TH* thalamus, *V* ventral

more medially within the middle cerebellar peduncle than the ventral fibres and travel along the lateral border of the ipsilateral dentate nucleus. Most of them end within the anterior lobe including its vermian, paravermian and hemispherical parts (Fig. 4f,g). Trajectories connected with these dorsal fibres are also successively traced upwards within the paramedial crus cerebri (Fig. 5a), the paramedial pontine tegmentum (Fig. 5b,c). Figure 5e–h show trajectories of the dorsal fibres within the pons, the middle cerebellar peduncle, and within the cerebellar white matter beneath the dentate nucleus. The medial transverse fibres between the two corticospinal tracts (Fig. 6d) are connected to the dorsolateral part of the prefrontal cortex (Fig. 6a) through the rostral posterior limb of the internal capsule (Fig. 6b) and through the ventromedial, ipsilateral crus cerebri (Fig. 6c). Another group of trajectories have been tracked from the ipsilateral temporal and occipital lobes (Fig. 6e), through the caudal part of the posterior limb of the internal capsule (Fig. 6f) and through the dorsolateral part of the crus cerebri (Fig. 6g) to the transverse fibres located within the pons laterally to the corticospinal tract (Fig. 6h). However, the most complete corticopontocerebellar path corresponds to projections from the pericentral cortex to the hemispherical parts of the cerebellar anterior lobe (HV-VIIA) through the ipsilateral, ventromedial crus cerebri and through the rostroventral transverse fibres. Therefore the pontine nuclei giving off ventral fibres are mainly connected to the orbitofrontal and prefrontal cortices, whereas the pontine nuclei giving off dorsal fibres receive more widespread cortical cortices including also the temporal and occipital cortices. Trajectories emanating from the temporal and occipital cortices merge along the corticospinal tract, they surround laterally, within the pons. However, there are many areas of entanglement amongst all the corticopontine fibres.

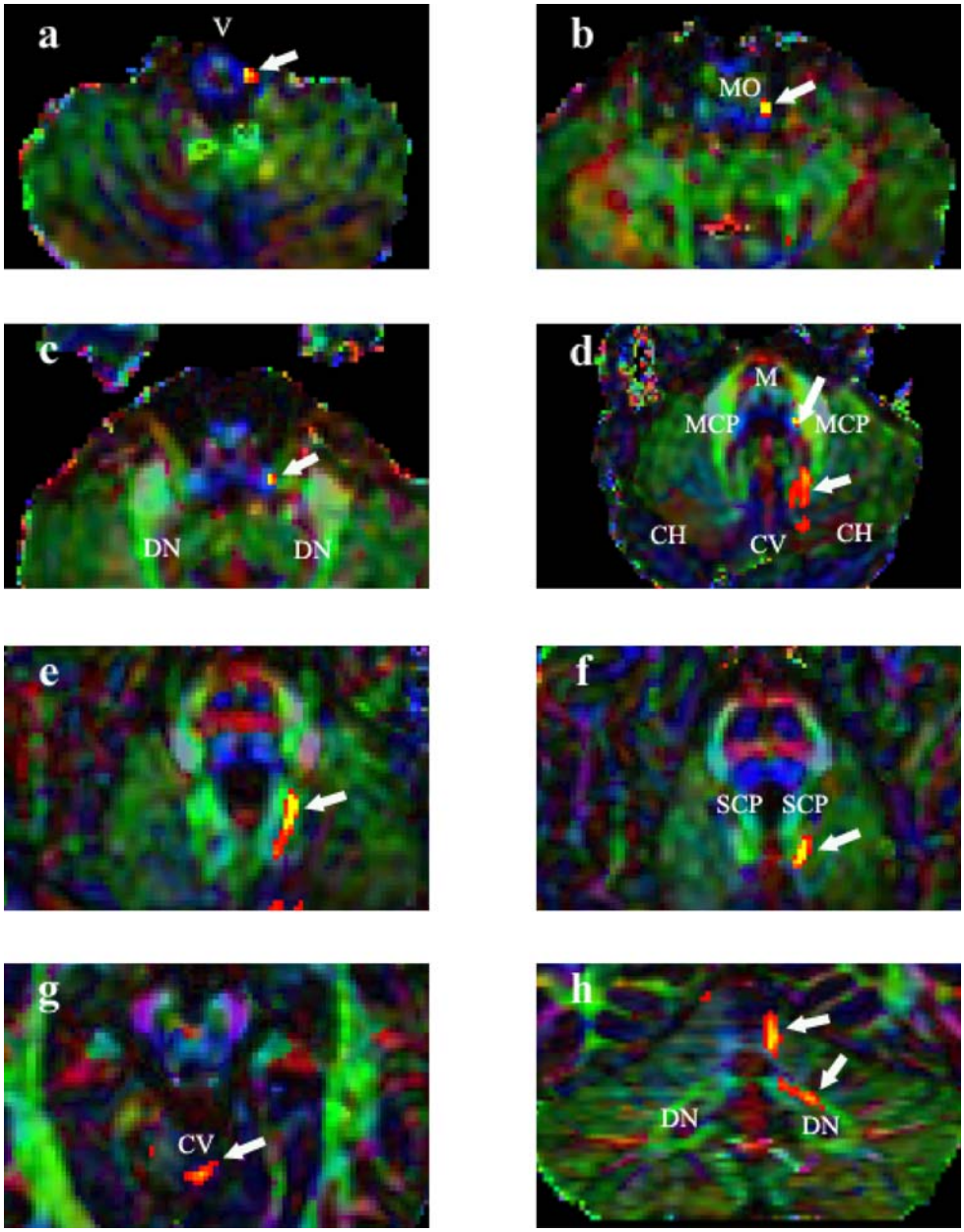

Fig. 3 Probabilistic mapping of inferior cerebellar peduncle. **a**–**c** View at the medullary level. **d** View at the pontine level. **e** View at the peridentate cerebellar white matter. **f** View at the supradentate cerebellar white matter. **g** View at the vermian part of the cerebellar anterior lobe. **h** Coronal view of the cerebellum. Well-delineated anatomic landmarks are labelled as follows: *CH* cerebellar hemisphere, *CV* cerebellar vermis, *DN* dentate nucleus, *M* mesencephalon, *MCP* middle cerebellar peduncle, *MO* medulla oblongata, *SCP* superior cerebellar peduncle, *V* ventral

The superior cerebellar peduncle

The dentatofugal course originates from the hilus of the dentate nucleus (Fig. 7a), runs within the superior cerebellar peduncle (Fig. 7b,c), goes through the mesencephalic tegmentum (Fig. 7d) and the red nucleus (Fig. 7e) and reaches the ventrolateral thalamus (Fig. 7f). Sometimes it gives off a thin descending tract within the dorsal and paramedial tegmentum, which may represent the ventral spinocerebellar tract.

The medial lemniscus

The course ascends within the rostromedial part of the medulla oblongata, dorsally and medially to the corticospinal tract (Fig. 8a,b). It spreads upwards, dorsal to the inferior olivary nucleus within the pontine tegmentum, ventral to the central tegmental tract (Fig. 8c,d). At the mesencephalic level, the course is located in a more ventrolateral position, dorsal to the substantia nigra and lateral to the red nucleus (Fig. 8e), and, at the telencephalic level, it terminates within the ventroposterior nucleus of the thalamus (Fig. 8f). Figure 8g is a medial view of the whole course of the medial lemniscus within the brainstem.

The corticospinal (and corticonuclear) tract

The computed course is successively followed from the most ventral part of the medulla oblongata in front of the inferior olivary nucleus (Fig. 9a) in the pons as a blue

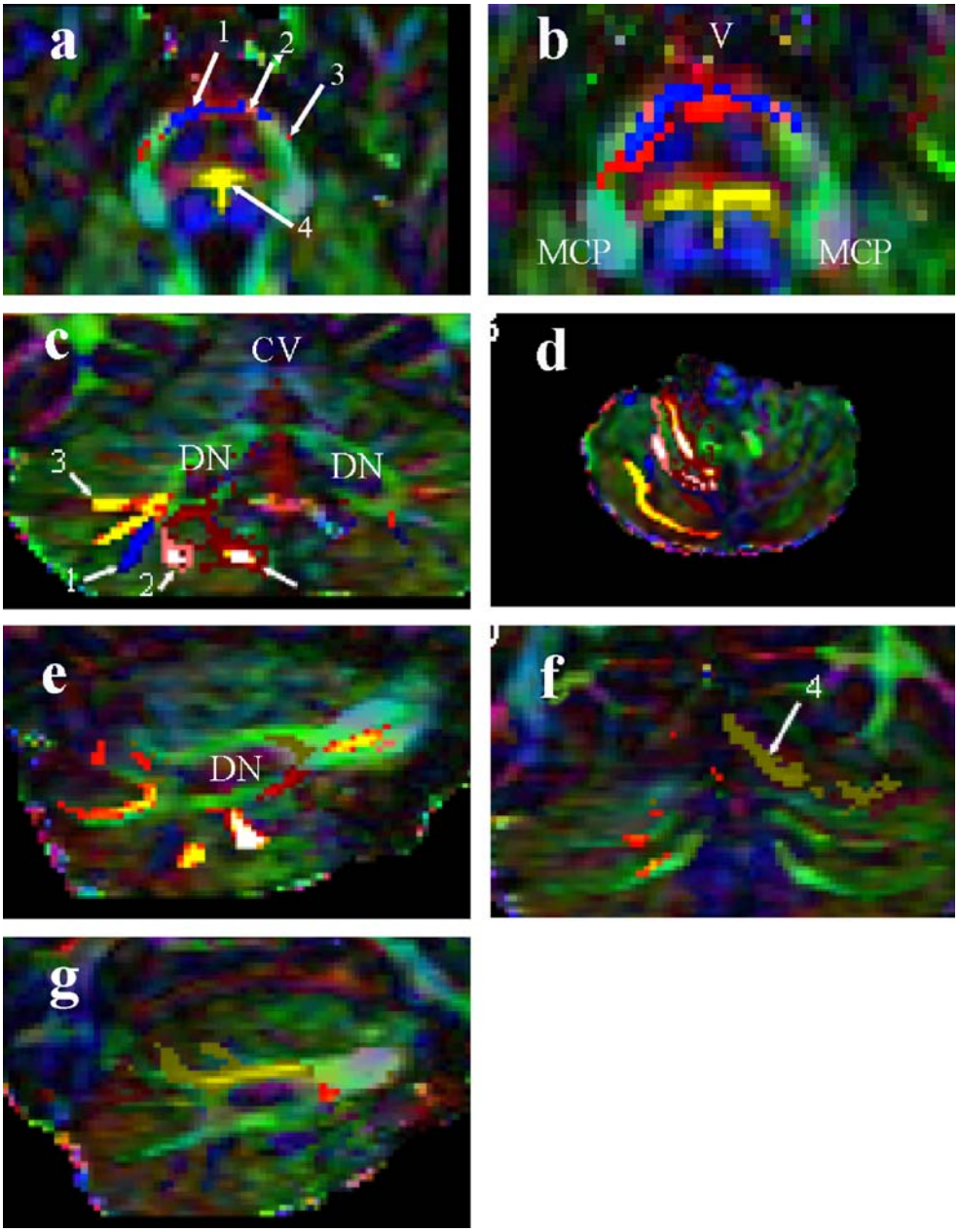

Fig. 4 Probabilistic mapping of pontocerebellar fibres from seed points located within ventral and dorsal transverse fibres. **a**, **b** Pontine level. **c** Coronal slice through the mid-cerebellum. **d** Axial slice through the cerebellar posterior lobe. **e** Medial slice through the cerebellum showing trajectories emanating from the posterior lobe. **f** Posterior coronal slice passing through the cerebellum showing trajectories (*4*) ending within the anterior lobe. **g** Medial slice passing through the cerebellum showing trajectories (*4*) travelling above the dentate nucleus. Well-delineated anatomic landmarks are labelled as follows: *CV* cerebellar vermis, *DN* dentate nucleus, *MCP* middle cerebellar peduncle, *V* ventral (*arrows 1–4* see explanations in the text)

compact bundle surrounded by the red H-shaped transverse fibres (Fig. 9b,c), the ventromedial part of the crus cerebri (Fig. 9d), the caudal part of the posterior limb of the internal capsule (Fig. 9e,f) and the sensorimotor cortex (Fig. 9h).

The medial longitudinal tract (possibly)

A course is traced in a dorsomedial location within the medulla oblongata (Fig. 10a) and within the floor of the fourth ventricle (Fig. 10b–d), dorsal to the central tegmental tract. It runs very close to the superior cerebellar peduncle within the pontomesencephalic junction (Fig. 10d,e). However, it remains in the dorsal mesencephalon at the junction between the tectum and tegmentum. This tract seems to terminate in the medial subthalamic area. It is tempting to identify this tract as the medial longitudinal tract as it remains strictly confined within the dorsal and medial brainstem. The medial longitudinal tract is mainly composed of ipsilateral fibres and goes through associative fibres connecting oculomotor, vestibular, reticular and spinal nuclei. Of course, other tracts run in the same zone such as tectospinal fibres or fibres belonging to the raphe system. Therefore, it cannot be ruled out that this reconstructed path may include other thin and contiguous pathways. Moreover, this tract is very close to the more dorsal central tegmental tract and to the more ventral medial lemniscus, so that it could just represent a part of these

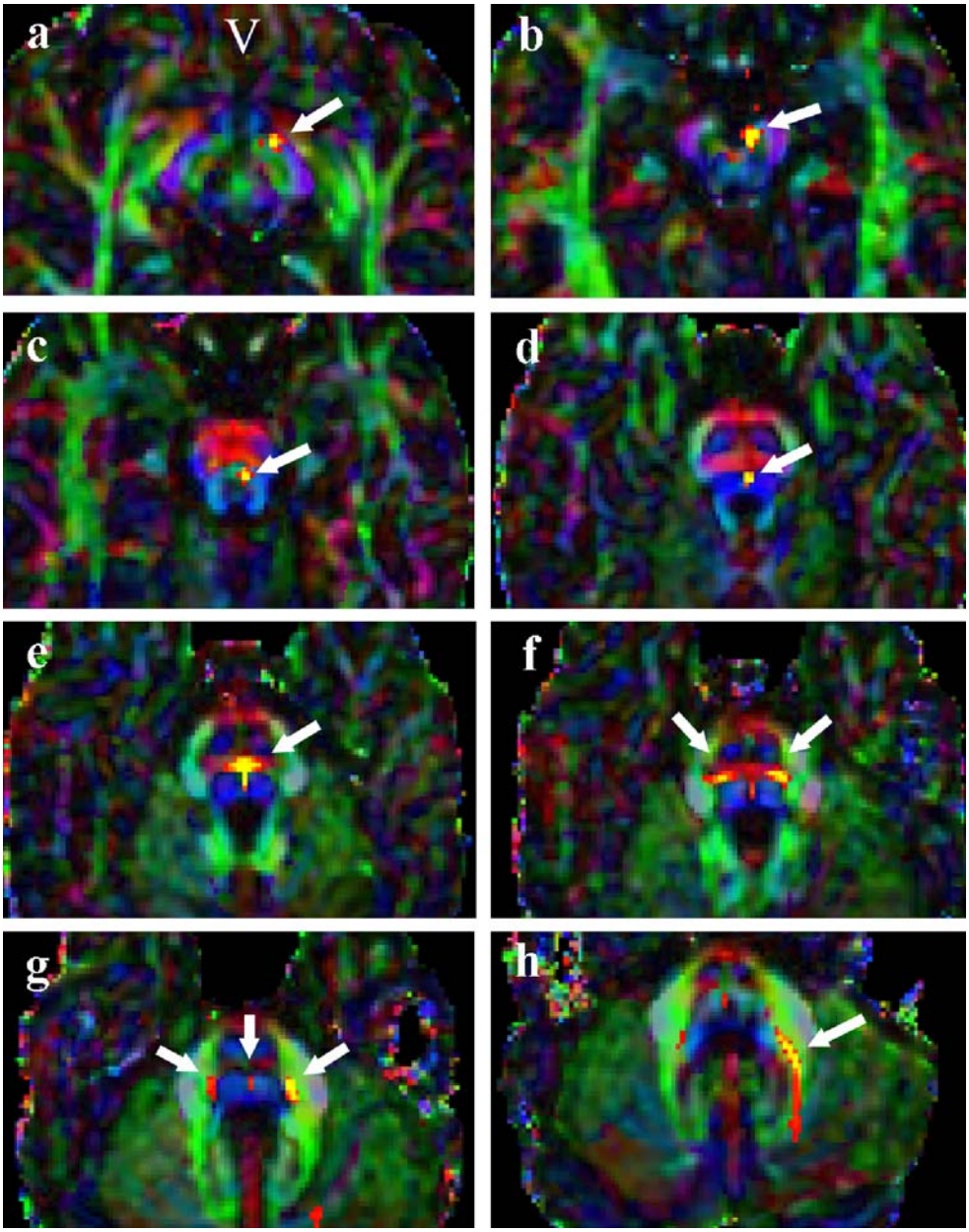

Fig. 5 Probabilistic mapping of corticopontocerebellar fibres. **a** View at the diencephalomesencephalic junction. **b** View at the mesencephalic level. **c**–**f** View at the pontine level. **g**, **h** Trajectories within the middle cerebellar peduncle and the peridentate cerebellar white matter. *V* ventral

latter bundles. However, this possibility seems to be unlikely as their respective tractograms display very distinct anatomic origins and targets for all of them.

The trigeminal system

The oblique course of the trigeminal nerve is traced within the mid-pons and outside within the prepontine cistern (Fig. 11a). This course takes a rostrocaudal direction within the most lateral floor of the fourth ventricle, lateral to the central tegmental tract and ventral to the inferior cerebellar peduncle (Fig. 11b,c). It may correspond to fibres arising from the pontine motor nucleus and to fibres terminating within the pontine principal nucleus. Trigeminothalamic fibres are known to be associated with the medial lemniscus so that they are not discriminated by the present tractography algorithm.

Figure 12 summarizes the main anatomical tracts directly discernible on the diffusion tensor coloured images from the mesencephalon (Fig. 12a) to the medulla oblongata (Fig. 12f), in agreement with the tractograms discussed above.

Discussion

The present study completes previous reports which dealt with the brainstem white-matter parcellation [1–6]. Several

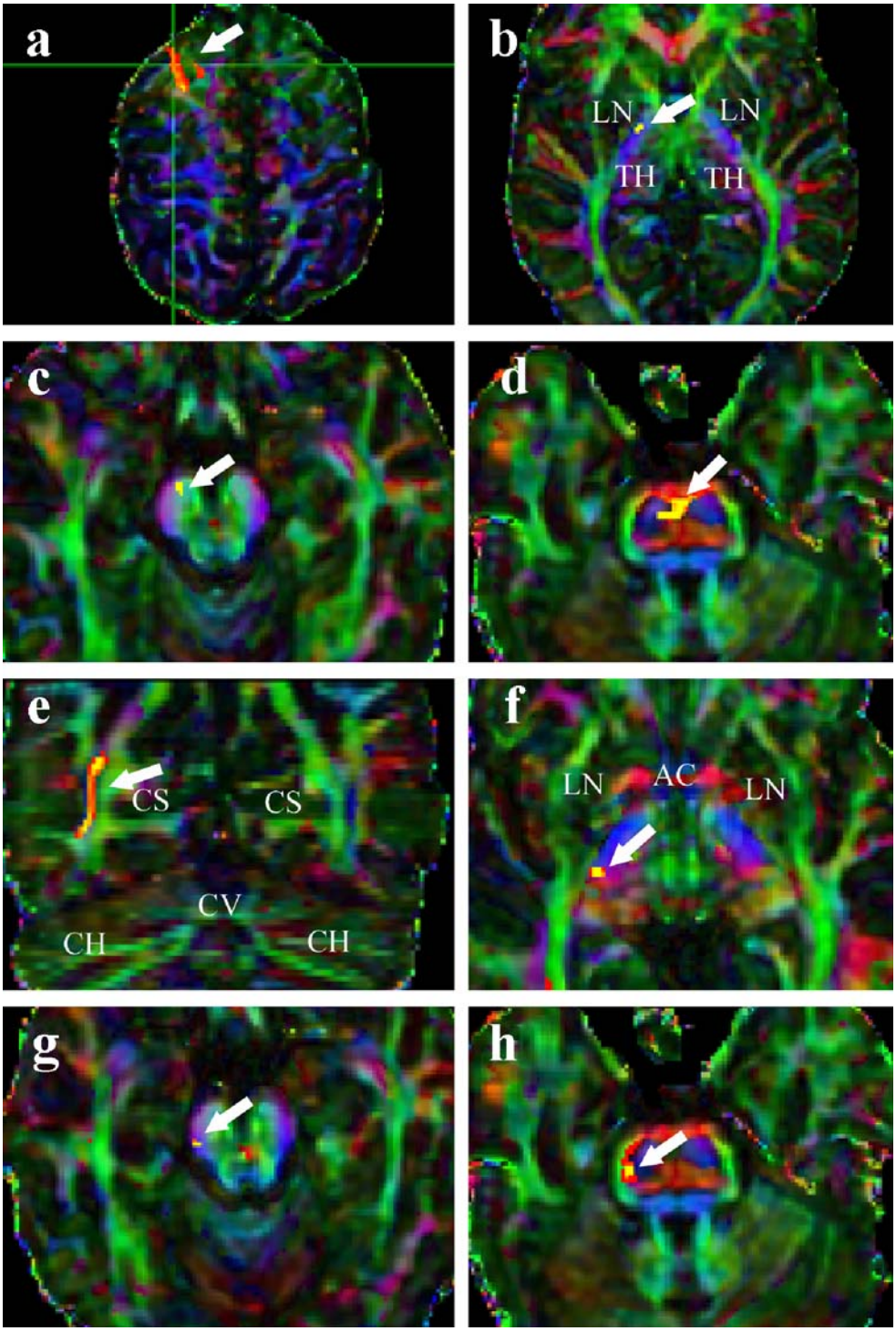

Fig. 6 Probabilistic mapping of corticopontine fibres originating in the prefrontal cortex (**a**–**d**), and in the temporal and occipital cortices (**e**–**h**). **a** Prefrontal level. **b** Diencephalic level within the posterior part of the internal capsule. **c** Mesencephalic level within the medial crus cerebri. **d** Pontine level between the corticospinal tracts (*blue*). **e** Temporooccipital white matter level. **f** Telencephalic level within the posterior part of the internal capsule. **g** Mesencephalic level within the dorsolateral part of the crus cerebri. **h** Pontine level within the lateral transverse fibres. Well-delineated anatomic landmarks are labelled as follows: *AC* anterior commissure, *CH* cerebellar hemisphere, *CS* calcarine scissure, *CV* cerebellar vermis, *LN* lentiform nucleus, *TH* thalamus

tracts such as corticospinal, corticopontine and central tegmental tracts, median lemniscus, and cerebellar peduncles, can be easily identified on the structural images and on reconstructed pathways using tractography. However, these computed trajectories may include other thinner tracts because of the low spatial resolution, and the possible entanglement with their paths. This problem may especially occur within the mesencephalic and the pontine tegmentum where different bundles are contiguous and parallel; for example, the lemniscus median and the neospinothalamic tract are tightly adjoined, and both end within the thalamus so that it is difficult to dissociate them for the moment. It is noteworthy that, although high fields increase susceptibility artefacts and correlative image distortions due to static field inhomogeneities, we acquired very few distorted images of the brainstem, partly due to parallel imaging (ASSET

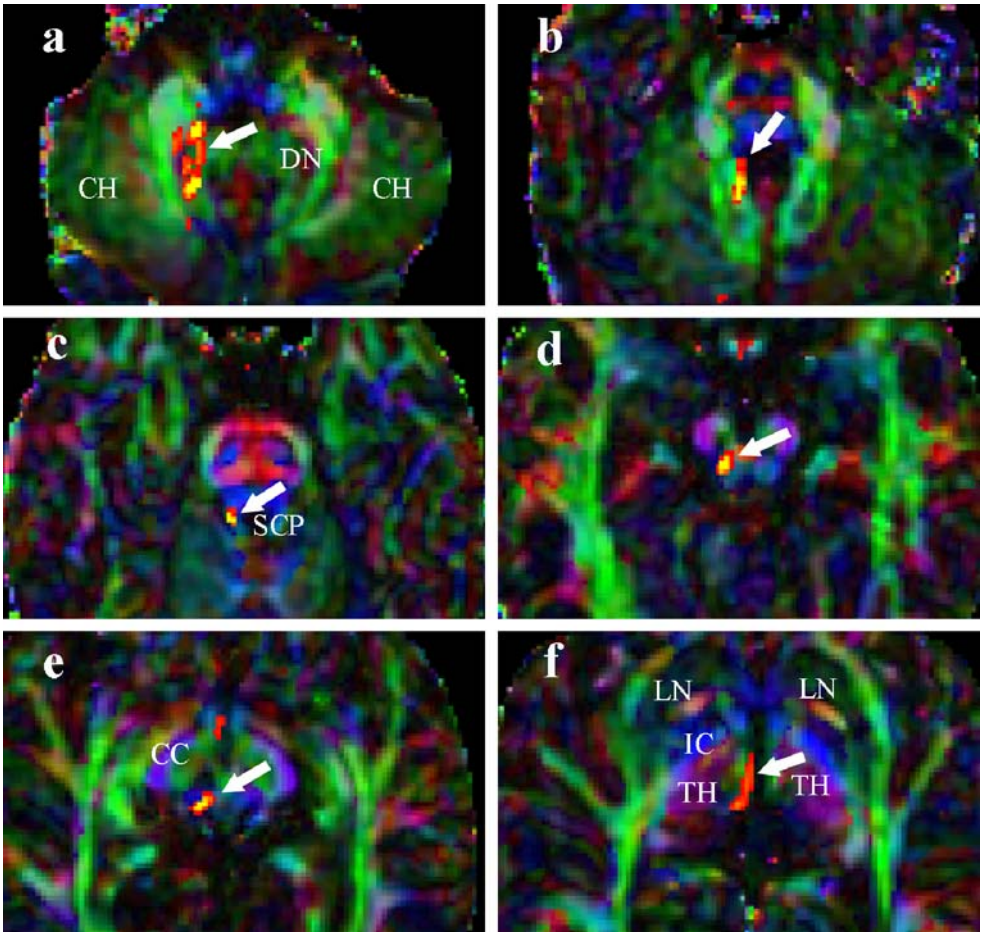

Fig. 7 Probabilistic mapping of superior cerebellar peduncle originating in the right dentate nucleus. **a**–**c** View at the ponto-cerebellar level. **d**, **e** View at the mesencephalic level within the retronigral ventral tegmentum. **f** View at the low diencephalic level. Well-delineated anatomic landmarks are labelled as follows: *CC* crus cerebri, *CH* cerebellar hemisphere, *DN* dentate nucleus, *IC* inferior colliculus, *LN* lentiform nucleus, *SCP* superior cerebellar peduncle, *TH* thalamus

option). In comparison with previous studies at 1.5 T [1–5], image quality at 3 T was quite equivalent but the spatial resolution was better.

Several factors could improve the sensibility and the specificity of DTI and tractography. First, it is possible, as we did in the present study, to increase the imaging matrix and the number of diffusion gradients, as well as to decrease the slice thickness. However, this results in a decrease in signal/noise ratio and a marked increase in examination duration. In order to maintain a high level of signal/noise ratio, it is necessary to increase the NEX, which again results in an increase in time (>20 min) and, consequently, impractical for routine clinical use. Based on our experience, we recommend for the brainstem: millimetric voxels, NEX at least 2, and between 30 and 55 diffusion gradients. The present results at 3 T with 55 gradient directions are mainly comparable with those in a previous study at 3 T with 30 diffusion gradients and the same imaging matrix [5]. With 55 gradient directions, several tracts, such as the superior cerebellar tract, are more easily delineated on colour-coded maps than with 30 gradient directions. However, even if these technical adjustments can help to dissociate very close fibres and to detect subtle direction modifications along broad parallel paths, they do not enable the main limitation of DTI, that is partial volume averaging, to be completely overcome.

In particular, a tricky problem is represented by fibre-crossing, by fibre-kissing and by collateralization within a voxel. To accounting for this complex fibre architecture at the voxel scale it is necessary to give up the DTI gaussian hypothesis and to apply model-free algorithms. New techniques, such as diffusion spectrum and q-ball imaging [11, 12], spherical deconvolution [13] and persistent angular structure [14], allow the main different diffusion orientations within the same voxel and supposed to correspond to fibre crossings to be determined. A recent study in monkeys [15] has shown good agreement between association fibre pathways in the brain, computed by diffusion spectrum imaging and the same pathways traced by autoradiography. Another method, called probabilistic diffusion tractography with multiple fibre orientations, has also recently been developed [16]. Instead of estimating the whole diffusion profile within each voxel in a model-free manner, this probabilistic algorithm relies on a Bayesian estimation to fit the parameters of a multicompartment model to the measured data for each voxel. In comparison

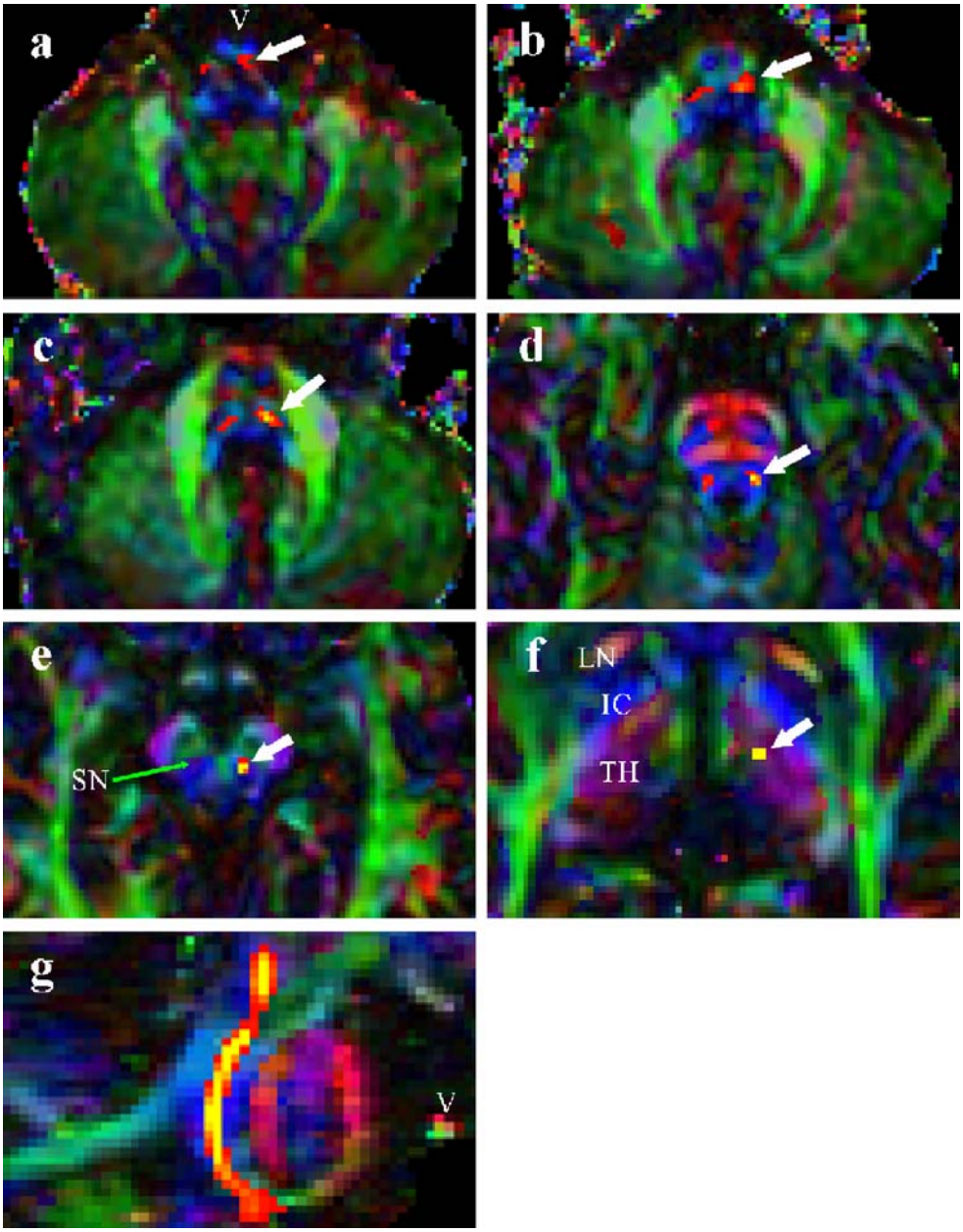

Fig. 8 Probabilistic mapping of the medial lemniscus. **a** View at the medullary level. **b**–**d** View at the pontine level. **e** View at the mesencephalic level within the ventral tegmental area. **f** View at the diencephalic level within the thalamus. **g** Paramedial view showing the medial lemniscus going through the whole brainstem. Well-delineated anatomic landmarks are labelled as follows: *IC* inferior colliculus, *LN* lentiform nucleus, *SN* substantia nigra, *TH* thalamus, *V* ventral

with the model-free algorithms, this technique is not limited by angular resolution which is a great advantage in detecting, for example, fibre kissing, and displays robustness to noise. Indeed, the whole diffusion profile within the same voxel may encompass noise and leads to false-positive pathways. Therefore, all these methods appear to be complementary and it can be recommended that, in the same study, tractograms launched from similar seeds but obtained with both probabilistic and model-free algorithms should be computed and compared.

Third, a single voxel should be used as a seed point rather than a multivoxel region of interest. Fourth, based on the known anatomy, multiple seeds located over different parts of the same tract should be used to reconstruct a given pathway because of possible erratic tracking due to noise. Ideally, the true pathway would correspond to the intersection of all reconstructed trajectories. In this regard, a triangulation analysis of tractography has been recently developed to identify overlap between tracts computed from distinct seeds [17]. Fifth, putative anatomical connectivity as computed by tractography could be compared to neural networks inferred from functional connectivity (fc) analysis. fcMRI copes with correlations between low-frequency BOLD signal fluctuations of different brain regions. These correlations are thought to reflect partly underlying anatomical connectivity [18]. Altogether, all

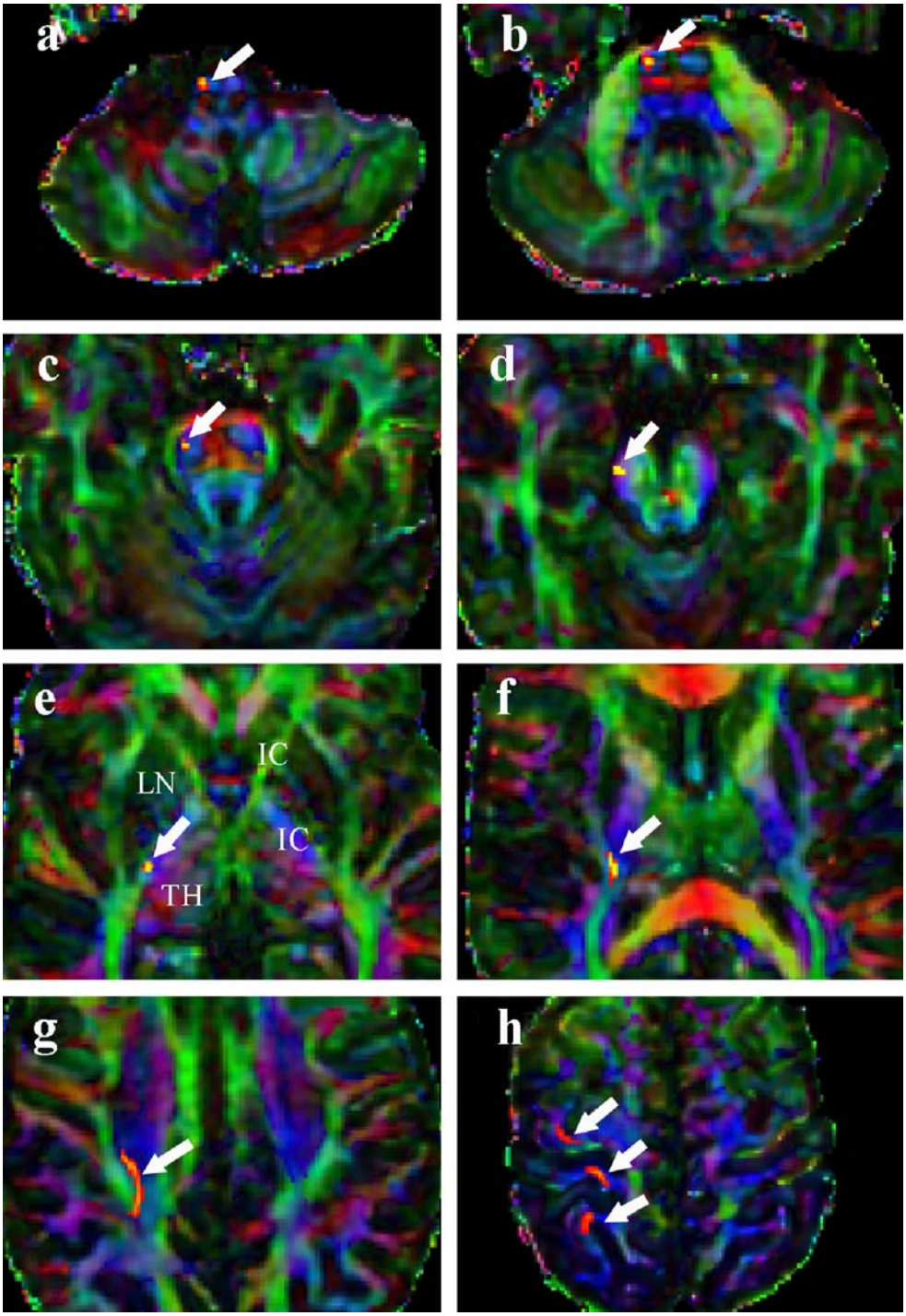

Fig. 9 Probabilistic mapping of the corticospinal (corticonuclear) tract. **a** View at the medullary level. **b**, **c** View at the pontine level. **d** View at the mesencephalic level within the medial crus cerebri. **e**, **f** View at the diencephalic level within the posterior part of the internal capsule. g View at the diencephalotelencephalic level within the anterior part of the internal capsule. **h** View at the view at the telencephalic level (sensorimotor cortex). Well-delineated anatomic landmarks are labelled as follows: *IC* inferior colliculus, *LN* lentiform nucleus, *TH* thalamus

these factors could improve the amount of discrimination of tractography for: (1) thin ascending and descending tracts, such as the lateral lemniscus or tectospinal tract, and (2) transverse fibres, such as cranial nerves or reticular association fibres. The main limitation of our present results is that the probabilistic algorithm we used does not estimate all the dominant diffusion directions within the same voxel.

In the present study, four results must be emphasized. First, the central tegmental tract is clearly delineable and must be distinguished from the median lemniscus which lies more ventrally within the pontine tegmentum, and more ventrolaterally within the mesencephalic tegmentum. We also show that corticoolivary fibres issuing from prefrontal areas travel downwards, especially between the main dorsal and paramedial components within the floor of the fourth

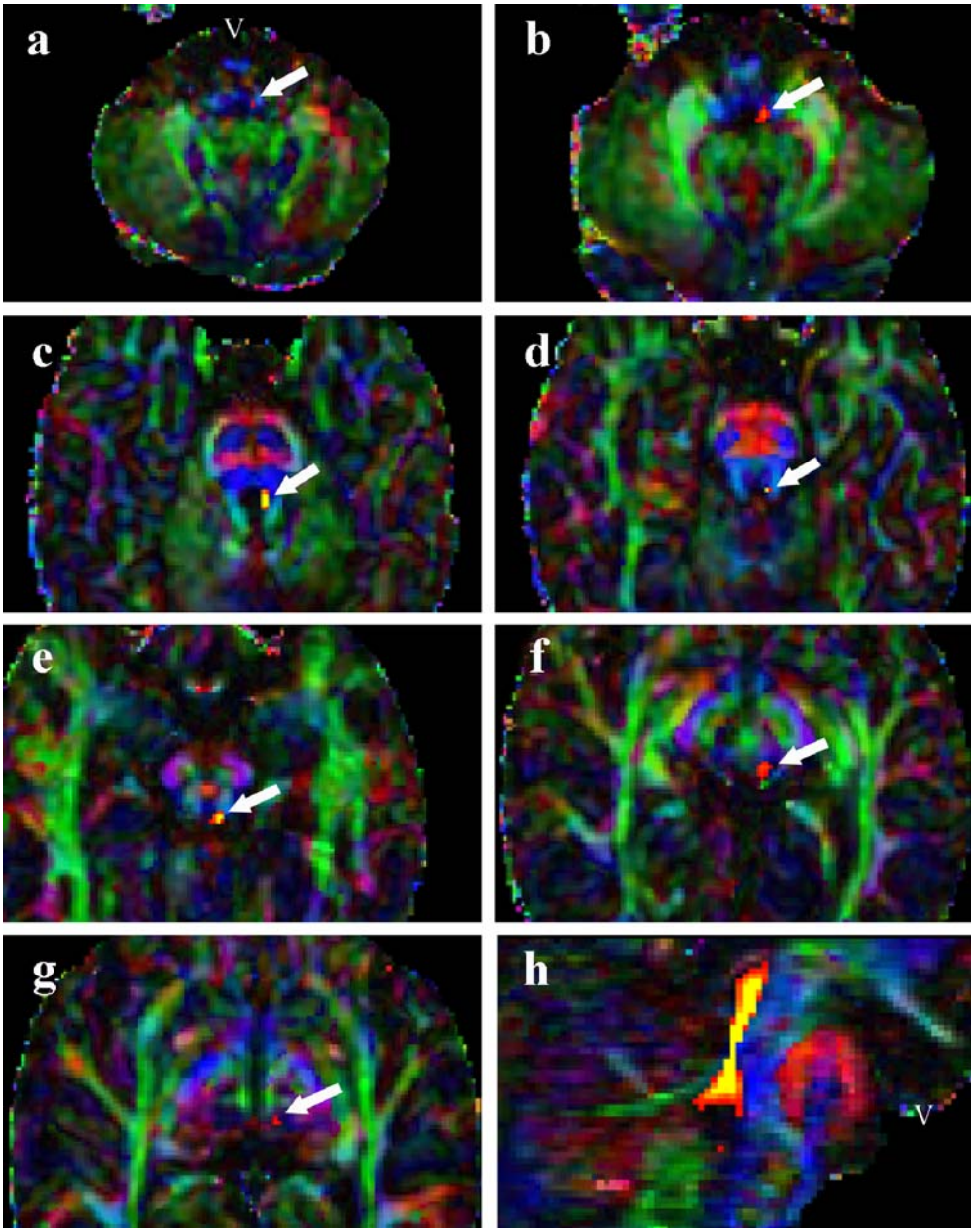

Fig. 10 Probabilistic mapping of a dorsomedial tract: putative medial longitudinal fibres. **a**, **b** View at the medullary level. **c**, **d** View at the pontine level close to the superior cerebellar peduncle. **e**, **f** View at the mesencephalic level within the tegmentotectal area. **g** Mesencephalo-diencephalic junction. **h** Paramedial view showing these fibres running through the whole brainstem. *V* ventral

ventricle (rubroolivary fibres [6]). Moreover, this result proves that all the relays of the cerebellar–rubroolivary–cerebellar loop receive neocortical afferents and, possibly, cognitive modulation [19]. Second, we strove to segment as well as possible the corticopontocerebellar system. This is an important but very tricky problem since cortical projections through internal capsules and the crus cerebri to the pontine nuclei within the ventral pons follow a very obtuse angular course. The magnitude of this angle between oblique afferents to the pontine nuclei and their axial efferents, as transverse fibres converge dorsally within the middle cerebellar peduncle, prevents the tractography algorithm reconstructing the whole cerebropontocerebellar pathway. However, some trajectories may appear smoother and less obtuse as we were able to track some cortico-pontocerebellar fascicles. First, transverse fibres constitute an H-shaped area surrounding the corticospinal and cortico-nuclear tract on both sides within the ventral pons. This area is coloured red on axial structural images as its fibre component mainly comprises laterolateral fibres, and is itself surrounded ventrally and laterally by ventrodorsal fibres, i.e. converging transverse fibres to the cerebellum. This H-shaped area has been subdivided in the monkey into subsets of pontine neurons according to their topography and their specific cortical afferents [20, 21].

The ventral pons is composed of rostral peduncular, median, paramedian, ventral, lateral, dorsal and dorsolateral nuclei, as well as of the tegmental pontine reticular nucleus.

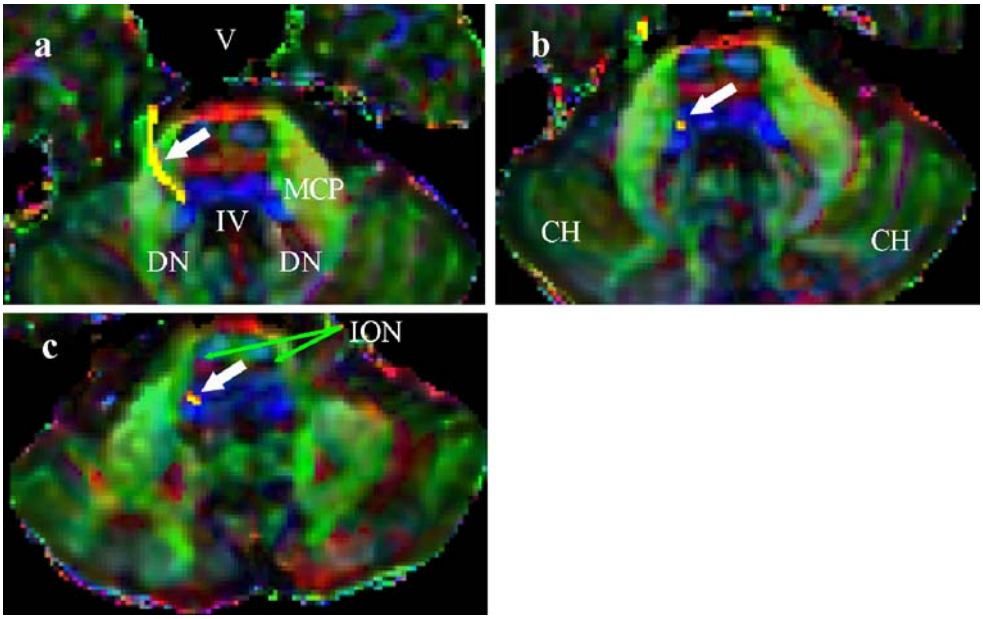

Fig. 11 Probabilistic mapping of the trigeminal nerve. **a**–**c** Views at the midpontine level. **a** Trigeminal nerve going through the middle cerebellar peduncle. **b**, **c** Part of the trigeminal complex within the dorsolateral pontine tegmentum. Well-delineated anatomic landmarks are labelled as follows: *CH* cerebellar hemisphere, *DN* dentate nucleus, *ION* inferior olivary nucleus (especially the principal nucleus), *IV* fourth ventricle, *MCP* middle cerebellar peduncle, *V* ventral

In the present study, we found that prefrontopontine fibres preferentially terminate within the medial and dorsal parts of the pons, whereas temporooccipital fibres end in lateral and dorsolateral parts of the pons. Some medial fibres bend ventrally and travel within the most ventral pons before joining the middle cerebellar peduncle. It is noteworthy that some computed trajectories issued from the neocortex terminate within the dorsomedial transverse fibre region and in the immediately more dorsal tegmental area. This area could correspond to the pontine tegmental reticular nucleus which receives neocortical afferents and projects to the cerebellum through the middle cerebellar peduncle [8, 9]. These results are in broad agreement with data obtained in the monkey displaying strong projections from the prefrontal cortex (Brodmann areas 8, 9, 10, 45 and 46) to the paramedian, median, peripeduncular, dorsomedial and reticular tegmental pontine nuclei, and from the temporal areas to the dorsal, dorsolateral and lateral nuclei. Cortical projections to the ventral pontine nuclei are mainly represented in the monkey by pre- and postcentral fibres. These data are on line with ours concerning the rostroventral transverse fibres [19].

Whenever seed masks were located over the caudoventral pontine region with a threshold of more than 30 samples, no fibres were tracked upwards within the mesencephalon and the brain because of the geometrical features of the corticopontine projections described above. However, when a very low threshold (fewer than 30 samples) was applied, few trajectories were observed within the medial crus cerebri and the posterior limb of the internal capsule broadly corresponding to the pericentral projections. Altogether, it seems that caudoventral transverse fibres may include intermingled fibres originating from pontine ventral and medial nuclei conveying few pericentral outputs and prominent prefrontal outputs. Of course, this broad parcellation of the pontine nuclear territory overlaps with corticopontine terminal fields. Moreover, we tried to identify precisely the cerebellar targets of the transverse fibres in terms of the function of their origin and their cortical afferents. The cerebellar anterior lobe is mainly connected to the sensorimotor cortex and the prefrontal cortex through rostroventral and medial pontine nuclei, respectively. Mossy fibres from the inferior cerebellar peduncle also terminate within the anterior lobe including the vermis. Conversely, the cerebellar posterior lobe receives its main connections from the prefrontal, frontoparietal and temporooccipital cortices through dorsomedial, ventral and lateral pontine nuclei, respectively, except from lobule IX which is linked to the inferior cerebellar peduncles. It is noteworthy that only mossy fibres terminating in the granular layer of the cerebellar cortex have seemingly been tracked. Climbing fibres from the inferior olivary nucleus as well as collaterals of mossy and climbing fibres ending in the deep cerebellar nuclei have not been visualized, probably because of their low density and their divergent topology in comparison with dense and compact pontocerebellar bundles.

The third finding we emphasize is that previous studies [4, 5] ascribed an erroneous localization to the decussation of the superior cerebellar peduncles. This decussation was situated within a region belonging to the mesencephalic tegmentum immediately caudal to the red nucleus and containing laterolateral fibres (depicted as a red area on the colour-coded maps). However, when this region is seeded, the resulting tractogram corresponds to the central tegmental tract. Of course, it cannot be ruled out that this

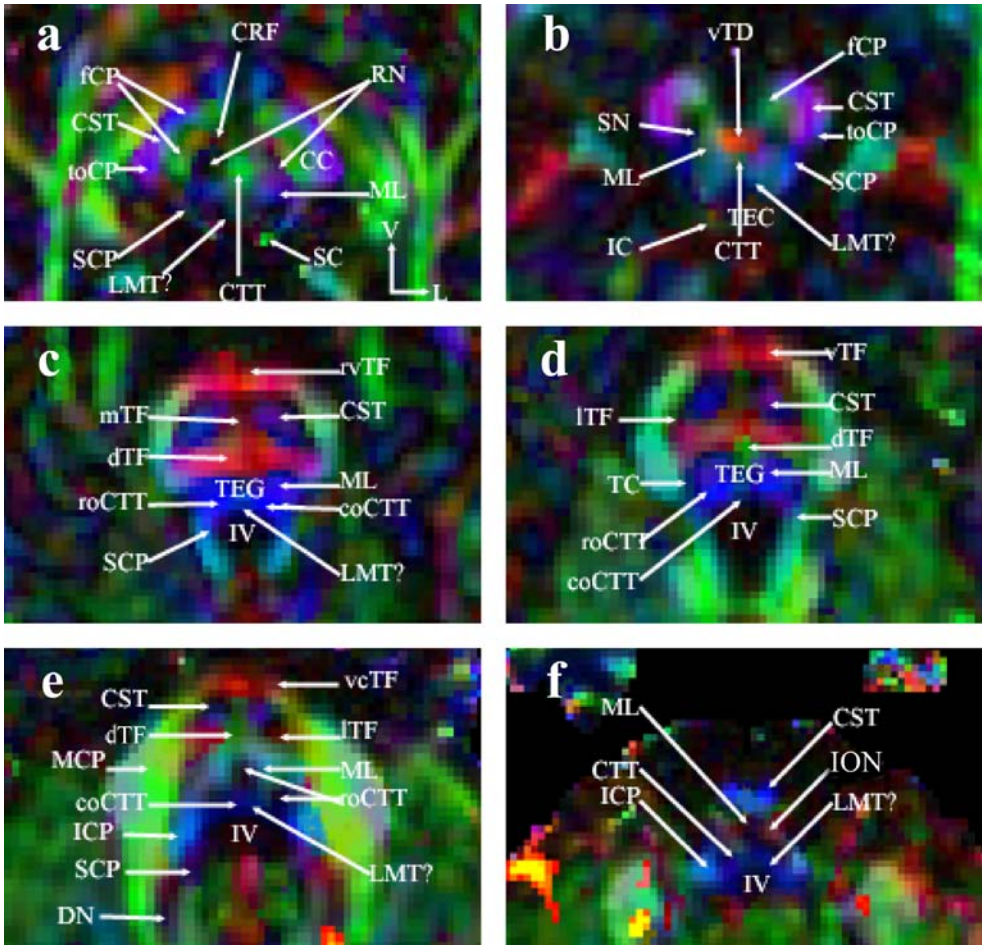

Fig. 12 Axial diffusion tensor imaging coloured maps recapitulating the location of the main tracts running within the brainstem. **a**, **b** Mesencephalon. **c**–**e** Pons. **f** Medulla oblongata. Well-delineated anatomic landmarks are labelled as follows: *CC* crus cerebri, *coCTT* corticoolivary component of the central tegmental tract, *CRP* cortico-rubral fibres (mainly from prefrontal cortex), *CST* corticospinal tract (including a corticonuclear component), *CTT* central tegmental tract, *DN* dentate nucleus, *dTF* dorsal transverse fibres (mainly connected to prefrontal fibres), *fCP* frontal fibres of the cerebral peduncle, *IC* inferior colliculus, *ICP* inferior cerebellar peduncle, *IOC* inferior olivary nucleus (especially the principal nucleus), *IV* fourth ventricle, *L* lateral, *LMT?* putative longitudinal medial tract, *lTF* lateral transverse fibres (mainly connected to temporooccipitocortical fibres), *MCP* middle cerebellar peduncle, *ML* medial lemniscus, *mTF* medial transverse fibres, *RN* red nucleus, *roCTT* rubroolivary component of the central tegmental tract, *rvTF* rostroventral transverse fibres (mainly connected to the sensori-motor cortical fibres), *SC* superior colliculus, *SCP* superior cerebellar peduncle, *SN* substantia nigra, *TC* (part of the) trigeminal complex, *TEC* tectum, *TEG* tegmentum. *toCP* temporooccipital fibres of the cerebral peduncle, *V* ventral, *vcTF* ventrocaudal transverse fibres (a major proportion of them consist of efferents of medial and dorsal pontine nuclei connected to prefrontal fibres), *vTD* ventral tegmental decussation beneath the overlying red nucleus, *vTF* ventral transverse fibres

tractogram may include crossed rubrospinal fibres but, in humans, the rubrospinal tract is either vestigial or absent [22]. Therefore, what was previously regarded as the decussation of the superior cerebellar peduncles more likely corresponds to the ventral mesencephalic decussation. The decussation of the superior cerebellar peduncles is located more caudally to the ventral mesencephalic decussation where these peduncles apparently cross the midline due to fibre-kissing [6]. Comparisons between colour-coded maps and a fibre atlas to identify tracts must, therefore, be interpreted with caution, and tractograms must be generated as often as possible.

Fourth, we described pontocerebellar fibers as if they were transmitted from the pontine nuclei to the *ipsilateral* cerebellar middle peduncles. However, it was shown in monkeys that transverse fibers mainly travel from one side to the opposite side crossing the midline at the same rostrocaudal level as the neuron from which they originate [23]. In the present study, pontine transverse fibers are located on both sides of the ventral pontine midline so that pontocerebellar fibers, we studied, do arise at the opposite side of their cerebellar target. It ensues that a strictly ipsilateral pontocerebellar pathway must be due, here again, to false tracking. The algorithm may have tracked the

contralateral homologous transverse fibers passing close to the pontine nuclei of the opposite side.

In conclusion, we describe several brainstem tracts, such as the central tegmental tract or medial longitudinal tracts, not previously displayed in a fibre tract brain atlas, or clearly delineated, and we give preliminary results concerning the broad anatomic delineation of the cortico-pontocerebellar pathways. As discussed above, future finer anatomical mapping of the brainstem and the cerebellar pathways will require the use of powerful techniques such as diffusion spectrum imaging, and the resulting tractograms to be compared with complementary results obtained with other imaging modalities such as functional connectivity.

Conflict of interest statement We declare that we have no conflict of interest.

References

1. Wakana S, Jiang H, Nagae-Poetscher LM, van Zijl PCM, Mori S (2003) Fiber tract-based atlas of human white matter anatomy. Radiology 230:77–87
2. Golay X, Jiang H, van Zijl PC, Mori S (2002) High-resolution isotropic 3D diffusion tensor imaging of the human brain. Magn Reson Med 47:837–843
3. Widjaja E, Blaser S, Raybaud C (2006) Diffusion tensor imaging of midline posterior fossa malformations. Pediatr Radiol 36:510–517
4. Salamon N, Sicotte N, Alger J, Shattuck D, Perlman S, Sinha U, Schultze-Haakh H, Salamon N (2005) Analysis of the brain-stem white-matter tracts with diffusion tensor imaging. Neuroradiology 47:895–902
5. Nagae-Poetscher LM, Jiang H, Wakana S, Golay X, Zilj PCM, Mori S (2004) High-resolution diffusion tensor imaging of the brain stem at 3T. AJNR Am J Neuroradiol 25:1325–1330
6. Habas C, Cabanis EA (2006) Cortical projections to the human red nucleus: a diffusion tensor tractography study with 1.5-T machine. Neuroradiology 48:755–762
7. Behrens TEJ, Woolrich MW, Jenkinson M, Johansen-Berg H, Nunes RG, Clare S, Matthews PM, Brady JM, Smith SM (2003) Characterization and propagation of uncertainty in diffusion-weighted MR imaging. Magn Reson Med 50:1077–1088
8. Nieuwenhuys R, Voogt J, van Huijzen C (eds) (1988) The human central nervous system. A synopsis and atlas, 3rd revised edn. Springer, Berlin Heidelberg New York
9. Haines DH (2000) Neuroanatomy. An atlas of structures, sections and systems, 5th edn. Lippincott Williams & Wilkins, New York
10. Schmahmann JD, Doyon J, Toga AW, Petrides M, Evans AC (2000) MRI atlas of the human cerebellum. Academic Press, San Diego
11. Tuch DS (2002) Diffusion MRI of complex tissue structure. PhD thesis, Harvard-MIT
12. Tuch SD (2004) Q-ball imaging. Magn Reson Med 52:577–582
13. Tournier JD, Calamante F, Gadian DG, Connelly A (2004) Direct estimation of the fiber orientation density function from diffusion-weighted MRI data using spherical deconvolution. Neuroimage 23:1176–1185
14. Jansons KM, Alexander DC (2003) Persistent Angular Structure: new insights from diffusion MRI data. Dummy version. Inf Process Med Imaging 18:672–683
15. Schmahmann JD, Pandya DN, Wang R, Dai G, d'Arcueil HE, de Crespignyt AJ, Wedeen VJ (2007) Association fibre pathways of the brain: parallel observations from diffusion spectrum imaging and autoradiography. Brain 130:630–653
16. Behrens TEJ, Berg HJ, Jbabdi S, Rushworth MFS, Woolrich MW (2007) Probabilistic diffusion tractography with multiple fibre orientations: what can we gain? Neuroimage 34:144–155
17. Aron AR, Behrens TE, Smith S, Franck MJ, Poldrack RA (2007) Triangulating a cognitive control network using diffusion-weighted magnetic resonance imaging (MRI) and functional MRI. J Neurosci 27:6743–6752
18. Cordes D, Haughton VM, Arfanakis K, Carew JD, Turski PA, Moritz CH, Quigley MA, Meyerand ME (2001) Frequencies contributing to functional connectivity in the cerebral cortex in "resting-state" data. AJNR Am J Neuroradiol 22:1326–1333
19. Schmahmann JD, Pandya DN (1997) Anatomic organization and functional implications of the basilar pontine projections from prefrontal cortices in rhesus monkey. J Neurosci 17:438–458
20. Brodal P (1978) The corticopontine projection in the rhesus monkey: origin and principles of organization. Brain 101:29–36
21. Brodal P (1979) The pontocerebellar projection in rhesus monkey: an experimental study with retrograde axonal transport of horseradish peroxidase. Neuroscience 4:193–208
22. Massion J (1967) The mammalian red nucleus. Physiol Rev 47:383–436
23. Schmahmann JD, Rosene DL, Pandya DN (2004) Ataxia after pontine stroke: insights from ponto-cerebellar fibers in monkey. Annals of Neurology 55:585–589